Acervo||ISSN: 2237 - 8723 Vol 07, Issue 11||2025
https://doi.org/10.5281/zenodo.17713701

Electrochemical Synthesis of Nio_2/Moo_2 Nanocomposite: A Sustainable Catalyst for Carboxylic Acid Photo Degradation and Water Purification

Charan Kumar Hunsur Chandrashekar[1], Shilpa Rajegowda[2], Thejas Gopal Krishne Urs[4], Raghavendra Maddur Puttaswamy[3] and Harsha Muddegowda[1]*

[1]Department of Chemistry, PES College of Engineering, Mandya, India – 571401
[2]Department of Chemistry, GSSS College of Engineering, Mysuru, India – 570016
[3]Department of Microbiology, Govt. Science College (Autonomous), Hassan, India – 573201
[4]Department of Physics, PES College of Engineering, Mandya, India – 571401

Abstract

NiO_2/MoO_2 nanocomposites were electrochemically synthesized and characterized to evaluate their potential as sustainable photocatalysts. The nanocomposites were analyzed using UV-Visible spectroscopy, XRD, SEM, and EDAX. Photocatalytic activity was investigated through the volumetric degradation of carboxylic acids—acetic acid, chloroacetic acid, and trichloroacetic acid—in the presence of NaOH. The photocatalyst demonstrated a remarkable degradation efficiency of 97.8%. Photodegradation kinetics were analyzed, and the Taft Linear Free Energy Relationship (LFER) was applied to assess the reaction mechanism. Furthermore, the isokinetic temperature (β) for the oxidation of carboxylic acids was calculated to elucidate the thermodynamic aspects of the degradation process. The nanocomposite also demonstrated significant antibacterial activity against Bacillus subtilis (MTCC 441), Lactobacillus acidophilus (MTCC 447), and Staphylococcus aureus (MTCC 96). This study highlights the potential of NiO_2/MoO_2 nanocomposites as promising materials for environmental remediation, offering high photocatalytic efficiency and sustainable degradation of persistent pollutants.

Keywords: NiO_2/MoO_2nanocomposite, Carboxylic acids, LFER, Antibacterial activities

Introduction

Water pollution is a pressing global issue, with industrial and municipal effluents significantly contributing to the degradation of freshwater resources. Among the various contaminants, carboxylic acids—including acetic acid and haloacetic acids such as chloroacetic acid (CA) and trichloroacetic acid (TCA), which are commonly and abundantly present in freshwater sources [Villanueva CM et al., 2004]—are notable for their persistence and significant contribution to chemical oxygen demand (COD) and biological oxygen demand (BOD) in wastewater. These acids are also reported to be carcinogenic [Pan S et al., 2014] and toxic, making their removal critical to prevent bioaccumulation, ecological harm, and risks to human health.

Carboxylic acids are prevalent in wastewater from industries such as textiles, food processing, petrochemicals, and agricultural runoff. Additionally, CA and TCA are byproducts of chlorination processes used in water disinfection, further complicating water treatment efforts. Their toxicity, persistence, and bioaccumulative properties underscore the urgent need for innovative and sustainable solutions to mitigate their impact on aquatic ecosystems. Various methods have been explored to address these residues, including electrochemical techniques [Liu et al., 2022, Tung et al., 2006], chemical and biological processes [Tung et al., 2006], adsorption [Zhao et al., 2014], nanofiltration [Tang et al., 2013;

Punyapalakul et al., 2009], microbial degradation [Yang et al., 2017; McRae et al., 2004], and advanced oxidation processes [Behbahani et al., 2018]. Photodegradation, leveraging sunlight or ultraviolet (UV) light, has emerged as a promising technique for the degradation of organic pollutants, including carboxylic acids [Wang et al., 2009]. Recent advancements in nanotechnology have further revolutionized this field, with nanoparticles offering exceptional catalytic, electronic, and structural properties. Nickel and molybdenum compounds, particularly in oxide or sulfide forms, are widely employed as catalysts in diverse applications such as hydroprocessing, methanol oxidation, methane reforming, and dimethyl oxalate hydrogenation [Tari et al., 2018; Suriyaprabha et al., 2017; Lewis et al., 1992; Li et al., 2016; Brookes et al., 2014; Brookes et al., 2014; Majewski et al., 2013; Vidales et al., 2023; Mamatha et al., 2022; Bukkitgar et al., 2020]. Nickel and molybdenum compounds, particularly in oxide or sulfide forms, have gained significant attention due to their versatility in catalytic applications, including hydroprocessing, methanol oxidation, and methane reforming. This process is particularly effective for carboxylic acids because it facilitates the breakdown of these compounds into simpler, non-toxic molecules such as carbon dioxide and water. The ability to generate reactive species like hydroxyl radicals under photolytic conditions ensures targeted and efficient degradation, addressing both the persistence and environmental hazards posed by these acids. While sunlight-assisted photolysis offers a sustainable approach, UV-assisted methods are highly efficient, particularly when coupled with advanced catalysts. Recent studies have demonstrated the potential of nanocomposites to enhance the generation of reactive species, such as hydroxyl radicals, thereby accelerating the degradation of complex organic compounds into non-toxic byproducts. However, the quest for cost-effective and environmentally benign catalysts remains a critical challenge.

In this context, the electrochemical synthesis of NiO_2/MoO_2 nanocomposites represents a novel and sustainable approach to address these challenges. NiO_2/MoO_2 nanocomposites are renowned for their exceptional photocatalytic properties, stability, and tunable surface characteristics, making them ideal candidates for environmental remediation applications. These nanocomposites build upon the strengths of nickel-molybdenum alloys and oxides, which have demonstrated superior electrocatalytic performance in reactions such as the hydrogen evolution reaction (HER), oxygen evolution reaction (OER), and oxygen reduction reaction (ORR). For instance, nickel molybdenum oxides (NixMoy-oxide alloys) have shown remarkable activity and stability, particularly for HER and OER, and have been enhanced using innovative methods such as atomic layer deposition and electrochemical tuning [Uma et al., 2021; Manivel et al., 2015; Hu et al., 2024; Ma et al., 2018; Solomon et al., 2021; Videa et al., 2010; Sanches et al., 2004; Raj et al., 1990]. Furthermore, innovative synthesis methods, such as electrochemical tuning and atomic layer deposition, enhance their properties and extend their applicability to organic molecule oxidation. Compared to widely used photocatalysts like TiO_2 and ZnO, NiO_2/MoO_2 offers enhanced charge separation and broader light absorption, enabling more efficient degradation of complex organic pollutants under both sunlight and UV conditions. Additionally, the synergistic interaction between NiO_2 and MoO_2 minimizes recombination rates of charge carriers, a common limitation in traditional photocatalysts. The unique combination of nickel oxide (NiO_2) and molybdenum oxide (MoO_2) offers synergistic effects, including enhanced charge separation and improved light absorption, which are critical for efficient photodegradation under both sunlight and UV irradiation.

This study introduces the electrochemical synthesis of NiO_2/MoO_2 nanocomposites as a sustainable catalyst for the photodegradation of carboxylic acids. These nanocomposites leverage their unique structural and electrochemical properties, such as a high surface area and exceptional conductivity, to enhance the degradation of pollutants in environmentally friendly processes [Huang et al., 2001; Kondawar et al., 2011; Ma et al., 2002; Wei et al., 2009]. The research focuses on the degradation of acetic acid, DCA, and TCA, representing a range of carboxylic acids with varying structural complexities. By applying a NiO_2/MoO_2 nanocomposite synthesized via an electrochemical method, this study investigates the degradation kinetics in a NaOH solution, contributing valuable insights into the potential of these materials in photocatalysis and organic molecule oxidation. Unlike conventional methods, our approach integrates the advantages of electrochemical synthesis which allows for precise control over the nanocomposite's morphology and composition with the sustainability of photodegradation techniques. This dual approach not only targets the complete mineralization of carboxylic acids but also ensures minimal secondary pollution.

The novelty of this research lies in the combined application of NiO_2/MoO_2 nanocomposites for the degradation of haloacetic acids, a class of pollutants that are often resistant to conventional treatments. The synergistic properties of the nanocomposite, coupled with its scalable synthesis method, position it as a transformative solution for water purification. Furthermore, the study contributes to Sustainable Development Goal 6 (SDG 6) by advancing technologies for the sustainable management of water resources.

Beyond their photocatalytic applications, NiO_2/MoO_2 nanocomposites also demonstrate significant antibacterial activity, making them multifunctional materials for addressing both chemical and microbial contaminants in wastewater. These properties are particularly relevant in water purification systems, where microbial contamination poses a parallel challenge to organic pollutants.

This article also discusses the challenges and opportunities associated with the application of NiO_2/MoO_2 nanocomposites in real-world water treatment systems, addressing issues such as scalability, cost-effectiveness, and efficiency in pollutant removal, while drawing from recent advancements in nanotechnology and photocatalysis. The findings are expected to pave the way for innovative strategies to tackle persistent pollutants, thereby promoting cleaner and safer water for all.

Materials and methods

All chemicals used in the synthesis of the NiO_2/MoO_2 nanocomposite were of analytical grade. Nickel and molybdenum electrodes were procured from Alfa Aesar, while the platinum electrode was sourced from Elico Pvt. Ltd. Trichloroacetic acid, chloroacetic acid, and acetic acid were supplied by Loba Chemie Pvt. Ltd. All solutions were prepared using double-distilled water to ensure purity and consistency during the synthesis process. The optical properties of the synthesized NiO_2/MoO_2 nanocomposite were analyzed using a UV-Visible spectrophotometer (Shimadzu-1700 series). X-ray diffraction (XRD) analysis was conducted using a PANalytical X'Pert X-ray diffractometer with Cu Kα radiation ($\lambda = 1.54$ Å) over a scanning range of 0° to 80°. The morphological features of the nanocomposite were examined using scanning electron microscopy (SEM) coupled with energy-dispersive X-ray analysis (EDAX) on a Quanta-200 instrument (FEI, Netherlands). EDAX confirmed the elemental composition of the nanocomposite, identifying nickel (Ni), molybdenum (Mo), and oxygen (O) as its primary constituents.

Synthesis of NiO_2/MoO_2 nanocomposite by electrochemical method

The NiO_2/MoO_2 nanocomposite was synthesized via an electrochemical method using nickel (Ni) and molybdenum (Mo) electrodes in an aqueous $NaHCO_3$ solution. In this setup, the Ni and Mo electrodes served as the anode, while a platinum electrode was used as the cathode. The experiment was conducted at a current of 15 mA and a potential of 10 V for 2.5 hours, with continuous stirring. The experimental configuration is shown in Figure 1. The electrolytic cell contained a 5% $NaHCO_3$ solution, with the anode and cathode positioned 2 cm apart during electrolysis.

The resulting precipitates were filtered and thoroughly washed with double-distilled water to remove any organic residues or impurities. The wet powder was then dried at 750ºC in a muffle furnace to facilitate dehydration and eliminate $NaHCO_3$ impurities, yielding the NiO_2/MoO_2 nanocomposite. The electrochemical reaction rates for different metals vary based on their redox potentials; for instance, Ni has a redox potential of −0.257 V, while Mo has −0.20 V. Since the dissolution potential of Ni is more negative than that of Mo, NiO_2 formation occurs concurrently with MoO_2 formation, resulting in the synthesis of the NiO_2/MoO_2 nanocomposite. The reaction mechanism is depicted in Scheme 1.

$$Ni(s) \rightarrow Ni^{2+} + 2e^-$$

$$Mo(s) \rightarrow Mo^{x+} + xe^-$$

$$2NaHCO_3 + 2e^- \rightarrow 2CO_2 + 2Na^+ + 2OH^-$$

$$2H_2O + 2e^- \rightarrow H_2 + 2OH^-$$

$$Ni^{2+} + 2OH^- \rightarrow Ni(OH)_2$$

$$Ni(OH)_2 + OH^- \rightarrow NiO_2 + H_2O + e^-$$

$$Mo^{2+} + 2OH^- \rightarrow MoO_2 + H_2O$$

$$MoO_4^{2-} + 2H^+ \rightarrow MoO_2 + H_2O$$

Overall Reaction: $Ni(s) + Mo(s) + NaHCO_3 + H_2O \rightarrow NiO_2/MoO_2 + CO_2 + Na^+ + H_2$

Scheme 1. Plausible mechanism for the electrochemical synthesis of NiO_2/MoO_2

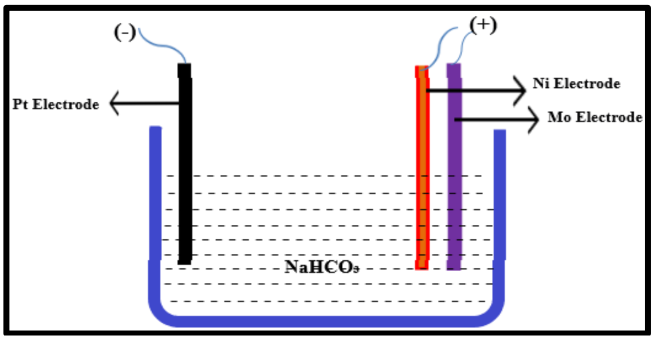

Figure 1. Experimental set up for the synthesis of NiO_2/MoO_2 nanocomposite.

RESULTS AND DISCUSSION

UV-Visible Spectra

The NiO_2/MoO_2 nanocomposite exhibits a maximum absorption peak at 300.91 nm in the UV region, as shown in Figure 2(a), with no significant absorption observed in the visible region. The optical band gap (E_g) was determined based on the fundamental absorption, corresponding to electronic transitions from the valence band to the conduction band. This was calculated using the Tauc relation:

$$(\alpha h\nu)^n \propto h\nu$$

where α is the absorption coefficient, ν is the photon energy, and $n = {}^1/_2$, for indirect transitions. By plotting $(\alpha h\nu)^{1/2}$ against hν and extrapolating the linear portion of the curve to intersect the hν axis at $\propto = 0$, the optical indirect band gap was determined [Rajput et al., 2024, Urs et al., 2017]. The band gap value, corresponding to the absorption edge, was calculated to be 3.83 eV, as shown in Figure 2(b).

The wide energy gap indicates that the NiO_2/MoO_2 nanocomposite is primarily suitable for UV-region-based applications, as the material's absorption properties restrict its efficiency in the visible spectrum. This characteristic highlights its potential for UV-driven photocatalytic processes, particularly in applications requiring high chemical stability and selectivity.

https://doi.org/10.5281/zenodo.17713701

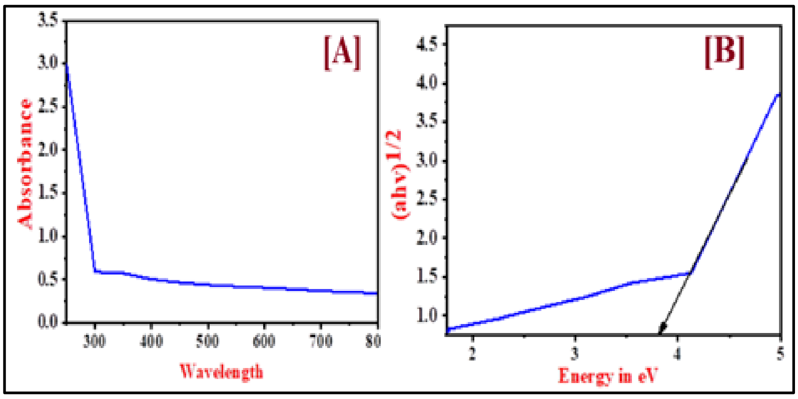

Figure 2. UV-Visible spectra and Tauc plot of NiO_2/MoO_2nanoparticles

Field Emission Scanning Electron Microscopy (FE-SEM)

This FE-SEM image depicts the surface morphology of a material characterized by a highly agglomerated structure, as shown in Figure 3. The enhanced resolution provided by FE-SEM reveals a rough and uneven surface, potentially increasing the material's surface area. At a magnification of 1.80k and a scale bar of 30 µm, the agglomerates are observed to be in the micron range, while individual particles are likely smaller, possibly within the nanometer range. The image also reveals inter-particle voids, contributing to the material's porosity.

Such porosity is advantageous for applications requiring efficient mass transfer, such as in electrochemical processes. If this image corresponds to a NiO_2/MoO_2 nanocomposite, the observed agglomeration may result from the synthesis method or interactions between the two oxides. The high-resolution imaging of FE-SEM allows detailed observation of this morphology, which can significantly influence key properties such as catalytic activity and adsorption capacity.

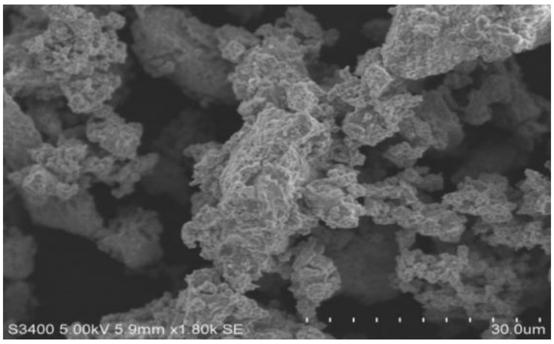

Figure 3. FE-SEM micrographs of NiO_2/MoO_2nanocomposites.

Energy Dispersive X-Ray Spectroscopy (EDS/EDX) spectrum

Figure 4 presents an Energy Dispersive X-Ray Spectroscopy (EDS/EDX) spectrum, a widely used technique for elemental analysis and chemical characterization of materials. The spectrum confirms the presence of nickel (Ni), molybdenum (Mo), and oxygen (O), aligning with the expected composition of the NiO_2/MoO_2 nanocomposite. The intensity of the peaks indicates that nickel and oxygen are the predominant components, while molybdenum is present in relatively smaller amounts.

The prominent oxygen peak is consistent with the formation of oxide compounds, further supporting the synthesis of a material containing nickel and molybdenum oxides. This EDS analysis provides strong evidence for the successful fabrication of the NiO_2/MoO_2 nanocomposite, highlighting its compositional elements and reinforcing its potential applications in catalytic and electrochemical systems.

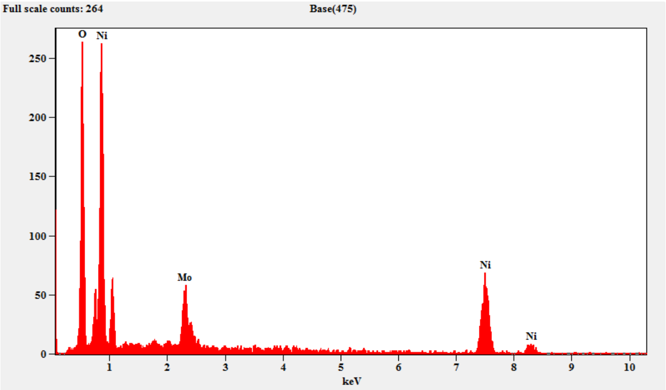

Figure 4. EDX of NiO$_2$/MoO$_2$nanocomposites

X-Ray Diffraction (XRD)

Figure 5 shows the XRD pattern of the synthesized NiO$_2$/MoO$_2$ nanocomposites. The diffraction peaks confirm the presence of mixed phases of NiO$_2$ and MoO$_2$. The prominent peaks observed at 2θ values of 33.02°, 38.30° 55.33°, 65.95° and 69.32° correspond to the (110), (101), (115), (135), and (026) crystal planes, respectively, of the NiO$_2$/MoO$_2$ nanocomposite. These diffraction peaks align well with the standard JCPDS card numbers **(NiO$_2$: 47-1049 and MoO$_2$: 65-5787)**, confirming the successful formation of the mixed-phase nanocomposite.

The XRD analysis further indicates that the nanocomposite exhibits a face-centered cubic (FCC) structure, as reflected by the positions and intensities of the diffraction peaks. The crystallite size was calculated using the Debye-Scherrer equation [Urs et al., 2014, Urs et al., 2016]:

$$D = \frac{k\lambda}{\beta \cos\theta}$$

where D is the average crystallite size, k is a shape factor with a value of 0.9, λ is the wavelength of the X-ray source (1.54 Å for Cu Kα radiation), β is the full width at half maximum (FWHM) of the diffraction peak, and θ is the angular position of the peak. The average crystallite size of the synthesized NiO$_2$/MoO$_2$ nanocomposite was found to be approximately 33.02 nm.

The XRD analysis clearly validates the successful synthesis of NiO$_2$/MoO$_2$ nanocomposites with well-defined crystallinity and phase composition. The presence of NiO$_2$ and MoO$_2$ phases, along with their consistent alignment to JCPDS standards, reinforces the reliability of the synthesis method and highlights the material's potential for catalytic and electrochemical applications.

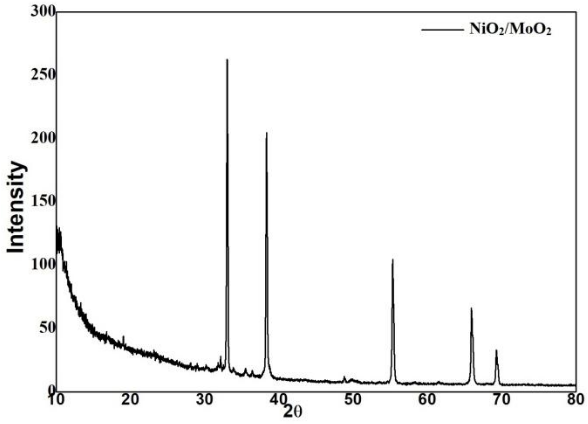

Figure 5. XRD patterns of NiO$_2$/MoO$_2$nanocomposite

Photodegradation Kinetics and COD Measurements

This study investigates the photodegradation of carboxylic acids—organic compounds characterized by the presence of a -COOH group—under light, particularly UV light. Photodegradation kinetics refers to the rate at which degradation occurs and examines how various factors, such as carboxylic acid concentration, catalyst loading, and temperature, influence this rate.

Chemical Oxygen Demand (COD), a key parameter in water quality analysis, measures the amount of oxygen required to chemically oxidize organic pollutants in water. In this study, COD serves as an indicator of the residual pollution following photodegradation, thereby providing a quantitative assessment of degradation efficiency.

The investigation focuses on the degradation behavior of carboxylic acids under light exposure, evaluating the roles of concentration, catalyst loading, and temperature in determining the photodegradation rate. Simultaneously, COD measurements are employed to quantify the reduction in organic pollutants, offering a comprehensive evaluation of the process's overall efficiency and its potential for environmental remediation.

Effect of concentration of carboxylic acids

Photodegradation experiments were conducted using carboxylic acid solutions of four different concentrations (ranging from 0.5×10^{-3} M to 3×10^{-3} M), while maintaining a constant weight of NiO_2/MoO_2 nanocomposites. The change in the concentration of carboxylic acids was monitored using a volumetric method, where the appearance of a pink color upon the addition of NaOH solution served as an indicator.

A plot of $\log(V/V_0)$ versus time exhibited linearity up to 60% of the reaction, indicating that the photodegradation of carboxylic acids follows first-order kinetics (Figure 6). The rate constant values, summarized in Table 1, reveal a decrease in the reaction rate as the acid concentration increases. This phenomenon can be attributed to the higher acid concentration intensifying the solution, thereby reducing the path length of photons penetrating the solution. As a result, fewer photons reach the catalyst surface, which diminishes the production of hydroxyl radicals and consequently reduces photodegradation efficiency.

To further evaluate the mineralization of the acid solution, Chemical Oxygen Demand (COD) values were monitored at various stages of the reaction. The formation of different radical species during the photodegradation process follows reaction pathways described in the literature [Shilpa et al., 2020; Ananda, S et al., 2014]. The photodegradation efficiency (η) of the photocatalyst was calculated using the following formula:

$$\eta(\%) = \frac{(C_0 - C_t)}{C_0} \times 100$$

Where: C_0 is the Initial concentration of the carboxylic acid (mg/L or M) and C_t is Concentration of the carboxylic acid at time t (mg/L or M).

Table 1. Results of photodegradation of carboxylic acids at varying concentrations, under UV light using NiO_2/MoO_2 nanoparticles (0.005g) at a temperature of 308K.

Catalyst 0.005g	**Carboxylic acids**	**Conc of acids in 10^{-3} M**	**10^3 k in sec^{-1}**	**COD Values in mg/L**		**Photodegradation Efficiency %**
				Before degradation	**After degradation**	
NiO_2/MoO_2 Nanoparti	Cl_3CCOOH	0.5	3.229	650	16	96.87
		1.0	1.356	640	16	96.74
		2.0	0.389	656	32	96.05
		3.0	0.189	624	16	95.06

	$ClCH_2COOH$	0.5	2.382	720	32	96.15
		1.0	1.115	752	16	97.72
		2.0	0.255	768	16	96.07
		3.0	0.150	784	48	95.16
	CH_3COOH	0.5	1.837	912	32	90.90
		1.0	0.689	880	48	97.05
		2.0	0.232	928	32	91.89
		3.0	0.139	912	32	95.23

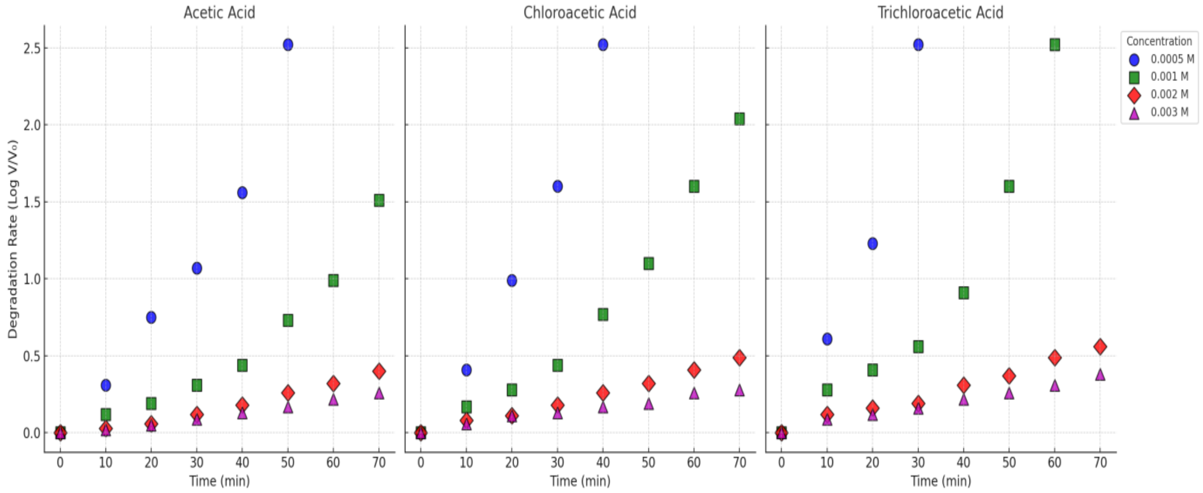

Figure 6. Effect of concentration of Carboxylic acids on the rate of degradation under UV light.

Effect of catalyst loading

Experiments were conducted by varying the catalyst loading from 0.002 g to 0.02 g while keeping the acid concentration constant. The photodegradation of carboxylic acids in the presence of a catalyst is significantly influenced by catalyst loading, as it determines the number of active sites available for the photocatalytic reaction.

At lower catalyst loadings, the limited number of active sites is insufficient to effectively degrade the carboxylic acids, resulting in lower degradation efficiency. As the catalyst loading increases, the number of active sites rises, enhancing photocatalytic activity and improving the degradation efficiency of carboxylic acids. However, beyond a certain threshold, further increases in catalyst loading lead to a decline in photocatalytic efficiency. This decline occurs due to the aggregation of catalyst particles at higher concentrations, which reduces the effective surface area and blocks the absorption of UV light.

Moreover, excessive catalyst loading can cause light scattering, decreasing the amount of UV light that penetrates the solution and reaches the catalyst surface. This limits the production of reactive species and diminishes the overall photocatalytic activity. Therefore, there is an optimal catalyst loading that maximizes the photodegradation efficiency by balancing the availability of active sites with the effective use of UV light.

In this study, the optimized catalyst loading was determined to be 0.005 g per 20 mL of solution (Figure 7 and Table 2). The corresponding Chemical Oxygen Demand (COD) values before and after degradation are summarized in Table 2, providing additional insights into the effect of catalyst loading on photo degradation efficiency.

https://doi.org/10.5281/zenodo.17713701

Table 2. Effect of catalyst loading on the photo degradation of carboxylic acids under UV light. The table presents the degradation efficiency (%), rate constants (10^3k in sec^{-1}), and COD values (before and after degradation) at varying catalyst loadings. [Acid concentration = 1.0×10^{-3} M; Temperature = 308 K]

Carboxylic acids	NiO_2/MoO_2 Nanoparticles	10^3 k in sec^{-1}	COD Values in mg/L		Photodegradation Efficiency %
			Before degradation	After degradation	
Cl_3CCOOH $1.0x10^{-3}$	0.002g	0.432	432	16	98.38
	0.005g	1.356	416	32	96.77
	0.01g	1.703	432	32	95.16
	0.02g	1.781	464	48	96.77
$ClCH_2COOH$ $1.0x10^{-3}$	0.002g	0.359	464	32	95.45
	0.005g	1.115	448	32	97.72
	0.01g	1.325	480	16	93.18
	0.02g	1.613	464	16	97.72
CH_3COOH $1.0x10^{-3}$	0.002g	0.319	368	48	94.11
	0.005g	0.689	384	32	91.17
	0.01g	0.959	384	48	94.11
	0.02g	1.155	368	48	97.05

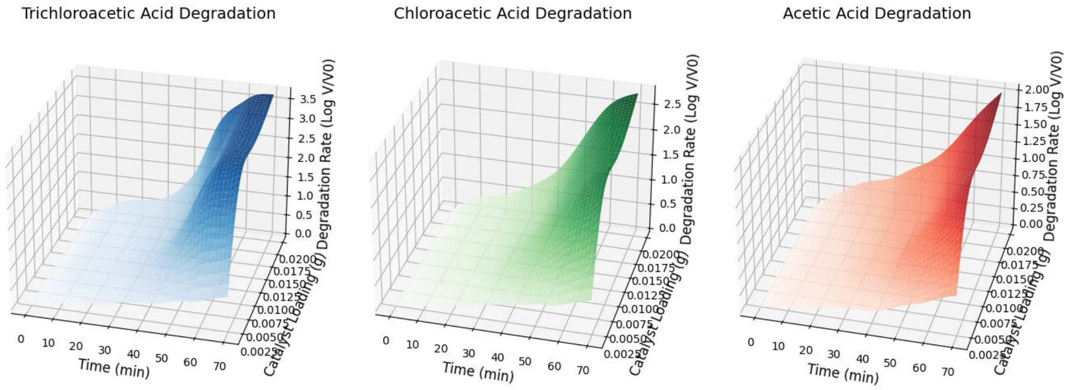

Figure 7. Effect of catalyst loading on the rate of degradation of carboxylic acids under UV light.

Effect of temperature

Temperature plays a critical role in influencing the rate of photodegradation, as it directly affects the reaction kinetics and diffusion rates of reactants. An increase in temperature typically enhances the degradation efficiency, a phenomenon attributed to several factors.

At higher temperatures, the diffusion rate of reactants within the solution increases, facilitating better interaction between the carboxylic acids and the catalyst surface. This increased molecular mobility leads to a higher frequency of effective collisions, thereby accelerating the photocatalytic reaction. Furthermore, elevated temperatures can enhance the generation of reactive oxygen species (ROS), such as hydroxyl radicals, which are vital for breaking down organic pollutants during photodegradation.

However, excessively high temperatures may negatively impact the reaction by causing catalyst deactivation or undesired side reactions, underlining the importance of maintaining an optimal temperature range for effective degradation.

The experimental results confirm that the photodegradation rate improves with temperature within the tested range. The rate constants and Chemical Oxygen Demand (COD) values, presented in Table 3 and Figure 8, respectively, highlight this trend. Additionally, thermodynamic parameters such as activation energy (E_a), enthalpy change (ΔH), and entropy change (ΔS) were calculated to provide further insights into the temperature dependency of the photo degradation process. These values are summarized in Table 4, offering a comprehensive understanding of the energy dynamics governing the reaction.

The findings emphasize the dual role of temperature in optimizing photodegradation efficiency while ensuring the stability and functionality of the catalyst under varying conditions.

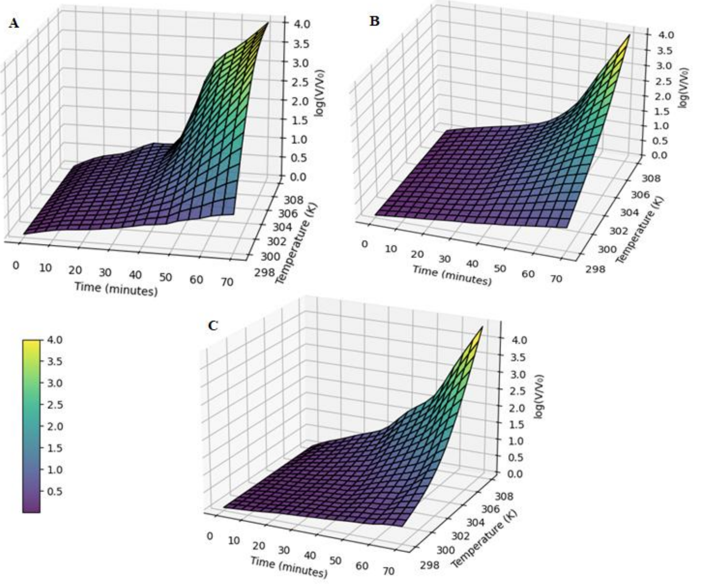

Figure 8. Effect of temperature on the rate of degradation of carboxylic acids under UV light [A] Cl_3CCOOH [B] Cl_3CCOOH [C] CH_3COOH

Thermodynamic Parameters for Photodegradation

The thermodynamic parameters calculated for the photodegradation of carboxylic acids provide insights into the energy dynamics governing the reaction. The enthalpy change ($\Delta H\#$) values confirm that the degradation process is endothermic, requiring an external energy input to proceed. Among the tested acids, CH_3COOH exhibited the highest $\Delta H\#$ (101.20 kJ/mol), indicating a greater energy requirement for activation compared to Cl_3CCOOH (59.76 kJ/mol) and $ClCH_2COOH$ (66.57 kJ/mol).

The negative entropy change ($\Delta S\#$) values across all samples indicate a decrease in disorder during the formation of the activated complex, which is characteristic of photodegradation reactions. However, the positive Gibbs free energy ($\Delta G\#$) values suggest that the process is thermodynamically non-spontaneous under ambient conditions (dark conditions without irradiation).

Despite this, photoexcitation compensates for this limitation by supplying the necessary energy to drive the reaction. When exposed to UV light ($\lambda < 400$ nm), the NiO_2/MoO_2 nanocomposite absorbs photons due to its bandgap energy of 3.83 eV, promoting electrons from the valence band to the conduction band. This transition generates electron-hole pairs (e^-/h^+), which subsequently interact with water molecules and dissolved oxygen to form reactive oxygen species (ROS), such as hydroxyl radicals (•OH). These ROS facilitate the oxidative breakdown of carboxylic acids, overcoming the inherent thermodynamic barrier.

The isokinetic temperature ($\beta = 307$ K), calculated from the linear correlation between $\Delta H\#$ and $\Delta S\#$, indicates that the reaction exhibits enthalpy-controlled behavior under experimental conditions (temperature range: 298–308 K). This suggests that higher temperatures enhance photodegradation efficiency by increasing molecular mobility and the frequency of reactive collisions between pollutants and ROS. The experimental confirmation of enhanced degradation rates at 308 K under UV irradiation further validates this photo-assisted compensation mechanism.

The activation energy (E_a) values also reinforce this trend, with CH_3COOH requiring the highest energy (103.72 kJ/mol) for degradation, consistent with its lowest photodegradation rate. This aligns with the observed first-order kinetics, where the reaction rate is highly dependent on light intensity and catalyst activation.

In summary, while the ΔG# values indicate thermodynamic non-spontaneity under dark conditions, the photoexcitation of NiO_2/MoO_2 nanocomposites compensates for this energy barrier by generating high-energy charge carriers (e^-/h^+) that drive photodegradation via ROS-mediated oxidation. This highlights the critical role of photoactivation in overcoming thermodynamic constraints and ensuring efficient pollutant degradation.

Table 3. Effect of temperature on the photodegradation of carboxylic acids under UV light using NiO_2/MoO_2 nanoparticles (0.005g). The table presents the degradation efficiency (%), rate constants (10^3k in sec^{-1}), and COD values (before and after degradation) for carboxylic acid solutions (1.0×10^{-3} M) at varying temperatures.

Carboxylic acids	**Catalyst 0.03g**	**Temperature in K**	**10^3 k in sec^{-1}**	**COD Values in mg/L**		**Photodegradation Efficiency %**
				Before degradation	**After degradation**	
Cl_3CCOOH $1.0x10^{-3}$	**NiO_2/MoO_2Nanocomposites**	298	0.476	368	16	98.38
		303	1.296	336	16	96.77
		308	1.356	336	32	98.38
$ClCH_2COOH$ $1.0x10^{-3}$		298	0.260	336	32	95.45
		303	1.105	336	32	97.72
		308	1.115	304	16	97.72
CH_3COOH $1.0x10^{-3}$		298	0.222	304	48	94.11
		303	0.405	288	16	97.05
		308	0.689	304	16	91.17

Table 4. Thermodynamic parameters for Carboxylic acids

Carboxylic acids	**$\Delta H^{\#}$** (kJ/mol)	**$\Delta S^{\#}$** (J/K)	**$\Delta G^{\#}$** (kJ/mol)	**E_a** (kJ/mol)	**E_a** (Cal/mol)
Cl_3CCOOH	59.76	-282.29	91.48	62.28	$14.886x10^3$
$ClCH_2CCOOH$	66.57	-282.11	92.0	68.36	$16.338x10^3$
CH_3COOH	101.2	-271.77	92.43	103.72	$24.7910x10^3$

https://doi.org/10.5281/zenodo.17713701

Structural Modification and Reactivity Analysis of Carboxylic Acids

Structural modifications of reactant molecules can significantly influence the rate or equilibrium constant of a reaction through polar, steric, and resonance effects. Among the various empirical models used to describe structure-reactivity relationships, linear free energy relationships (LFERs) are among the most successful and widely applied. In this study, experiments were conducted to establish an LFER for the oxidation/photodegradation of carboxylic acids using NiO_2/MoO_2 nanocomposites. The application of the Taft equation involved plotting log k against σ∗, yielding the following regression equation:

$$\mathrm{Log\,k} = 0.10\sigma^{*} - 3.06(\mathrm{r} = 0.993)$$

The positive value of the polar constant (ρ∗), though small, indicates that electron-donating substituents decrease the degradation rate. The observed order of degradation rates for the carboxylic acids is:

Trichloroacetic acid > Chloroacetic acid > Acetic acid.

The activation energy (E_a) was found to be highest for the slowest reaction and lowest for the fastest, demonstrating that the reaction is enthalpy-controlled. Furthermore, a linear relationship was observed between activation enthalpies ($\Delta H^{\#}$) and entropies ($\Delta S^{\#}$), and from the slope of the $\Delta H^{\#}$ versus $\Delta S^{\#}$ plot (r=0.993), the isokinetic temperature (β) was calculated to be 307 K.

This result was further validated using the Exner criterion [Exner et al., 1964]. A linear plot of $\log k_1$ at 303 K versus $\log k_2$ at 308K yielded a slope (b), and the isokinetic temperature was recalculated using the following expression [Shorter et al., 1978],

$$\mathrm{B} = \frac{\mathrm{T_2 T_1 (b - 1)}}{\mathrm{b(T_2 - T_1)}}$$

Here, k_1 and k_2 are the rate constants at temperatures T_1 and T_2 (with $T_2>T_1$), and b is the slope of $\log k_2$ against $\log k_1$. The recalculated β value was 317.73 K, slightly higher than the experimental temperature range, further confirming the enthalpy-controlled nature of the reaction. The significantly negative values of $\Delta S^{\#}$ suggest the formation of a rigid activated complex during the reaction. Additionally, the constancy of $\Delta G^{\#}$ values across the studied carboxylic acids indicates that oxidation/photo degradation proceeds via an identical mechanism [Bott et al., 1980].

Comparison of Photodegradation Rate Constants under UV Light and Sunlight

The photodegradation rate constant for the synthesized NiO_2/MoO_2 nanocomposites was evaluated under both UV light and sunlight. The results demonstrate that the rate constant is significantly higher under UV light compared to sunlight. This enhancement is attributed to the interaction of photon energy with the semiconductor material (NiO_2/MoO_2).

When a photon with energy greater than the band gap of the semiconductor interacts with it, an electron is excited from the valence band to the conduction band, leaving a corresponding hole in the valence band. These conduction band electrons and valence band holes (e^-/h^+) may either recombine, dissipating energy as heat, or become trapped in metastable surface states. These surface states interact with electron acceptors and donors adsorbed onto the semiconductor surface.

In the absence of suitable (e^-/h^+) scavengers, recombination typically occurs within a few nanoseconds, resulting in energy dissipation and reducing the photocatalytic efficiency. However, when appropriate scavengers are present, recombination is inhibited, allowing subsequent redox reactions to proceed. This mechanism highlights the effectiveness of NiO_2/MoO_2 nanocomposites as photocatalysts, particularly under UV light where the higher photon energy facilitates more efficient excitation and subsequent reactions.

https://doi.org/10.5281/zenodo.17713701

The degradation rate constant under sunlight, presented in Table 5, supports these findings and aligns with the observed energy band gap of 3.83 eV determined through UV-Visible spectral analysis. This band gap restricts significant activity under sunlight due to its lower photon energy compared to UV light, further emphasizing the superior performance of NiO_2/MoO_2 nanocomposites in UV-assisted photodegradation.

The comparative analysis of photodegradation under UV light and sunlight reveals a clear enhancement in degradation efficiency and rate constants for all three carboxylic acids Cl_3CCOOH, $ClCH_2COOH$ and CH_3COOH when exposed to UV light. This significant improvement is attributed to the higher photon energy of UV light, which exceeds the band gap of the NiO_2/MoO_2 nanocomposite (3.83 eV). As a result, the excitation of electrons from the valence band to the conduction band is more efficient, leading to a greater production of reactive species, such as hydroxyl radicals. These radicals play a critical role in breaking down the carboxylic acid molecules into less harmful byproducts.

The relationship between degradation rates and degradation times further highlights the superior performance of UV light, as demonstrated in Figures 9 and 10. Shorter degradation times under UV light, combined with higher rate constants, indicate that the photodegradation process is not only more efficient but also faster. The linear correlation between degradation rate constants and time suggests that the process is governed by first-order kinetics, consistent across the carboxylic acids. This reinforces the role of the NiO_2/MoO_2 nanocomposite as an effective catalyst for UV-assisted photodegradation, offering a promising solution for the removal of persistent pollutants from water.

Table 5. Effect of rate of degradation in sunlight and UV light.

Catalyst 0.01g	**Concentration of carboxylic acids in 0.001 M**	**Sunlight 10^3 k in Sec^{-1}**	**Time taken for 95% Degradation in min**	**UV light 10^3 k in Sec^{-1}**	**Time taken for 95% Degradation in min**
NiO_2/MoO_2 Nanocomposite	Cl_3CCOOH	0.535	140	1.356	60
	$ClCH_2COOH$	0.412	210	1.115	80
	CH_3COOH	0.237	260	0.689	100

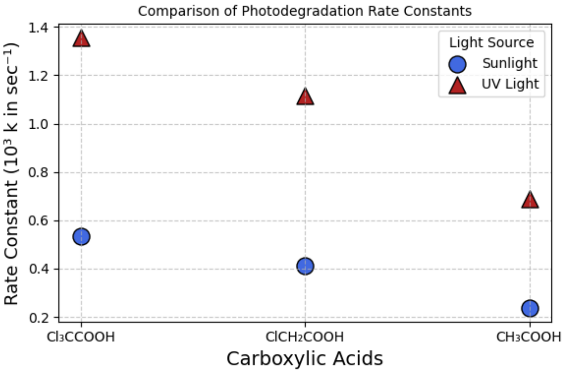

Figure 9. Comparison of photodegradation rate constants (10^3k) for carboxylic acids under UV light and sunlight using NiO_2/MoO_2 nanocomposites (0.01g).

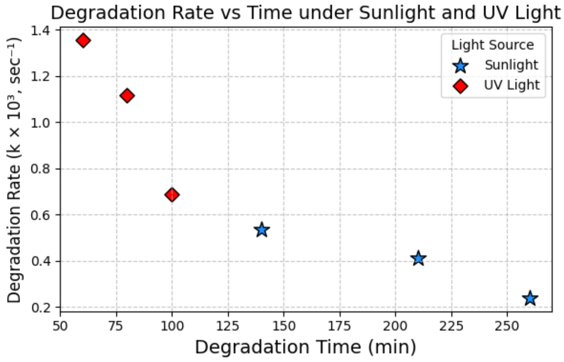

Figure 10. Relationship between degradation rate constants (10^3k, sec^{-1}) and degradation time (min) for carboxylic acids under sunlight and UV light.

Mathematical Modeling of Photodegradation Kinetics

Photodegradation of organic pollutants is a complex process influenced by multiple parameters such as time, catalyst loading, acid type, and reaction conditions. Developing a quantitative model for this process is crucial for optimizing reaction conditions and predicting degradation behavior under varying experimental setups. In this study, a polynomial regression model was developed to correlate the degradation rate with experimental parameters, providing a mathematical framework to interpret and predict photodegradation efficiency. A second-degree polynomial regression model was employed to capture the nonlinear dependencies of degradation rate on acid type, time, and catalyst weight. The acid type was considered as a categorical variable, where Acetic Acid was assigned a value of 1, Chloroacetic Acid a value of 2, and Trichloroacetic Acid a value of 3. The experimental time ranged from 0 to 70 minutes, and the catalyst weight was varied from 0.002 g to 0.02 g. The degradation rate was expressed in terms of Log V/V_0. Polynomial regression extends linear regression by incorporating quadratic terms to account for nonlinearities and interaction terms to model the combined effects of parameters. The final generalized polynomial equation obtained for degradation rate is:

$$\begin{aligned} D = {} & (-0.4077A) + (-0.0305t) + (-33.1003C_{cat}) + (0.0525A^2) + (0.0121A \times t) \\ & + (11.8799A \times C_{cat}) + (0.0004t^2) + (1.2157t \times C_{cat}) \\ & + \left(64.448 \times {C_{cat}}^2\right) + 0.6928 \end{aligned}$$

The results indicate that acid type significantly influences degradation efficiency, with trichloroacetic acid exhibiting the highest degradation rate compared to chloroacetic acid and acetic acid. The negative coefficient (-0.4077) for acid type suggests that the degradation efficiency progressively increases with the complexity of the acid structure. Catalyst weight plays a crucial role in degradation, as evidenced by the quadratic term (64.4481 for Catalyst Weight²), which has the highest magnitude among all coefficients. This indicates that catalyst loading is the most dominant factor affecting degradation efficiency. However, at higher catalyst concentrations, aggregation effects might reduce efficiency. The model also captures the effect of time on degradation, where the negative linear term (-0.0305) suggests that degradation slows down at longer durations, likely due to equilibrium effects or saturation of reactive sites. The interaction terms in the model provide further insights into degradation kinetics. The Time × Catalyst Weight interaction (+1.2157) highlights a synergistic effect, where increasing catalyst weight enhances the degradation rate as time progresses. Similarly, the Acid Type × Catalyst Weight interaction (+11.8799) suggests that different acids respond differently to catalyst concentration, necessitating catalyst optimization for each acid type.

The mathematical model was validated by training and testing on experimental data, ensuring robustness in predictions. The goodness-of-fit (R^2 value) confirmed that the model accurately represents the degradation trend, with experimental values closely matching predicted values.

The model also allows for the estimation of degradation rates under unseen conditions, making it a valuable tool for optimizing experimental setups. This equation enables predictions of degradation rates for any combination of acid type, time, and catalyst weight, providing a basis for experimental planning and reaction optimization. The ability to estimate the optimal catalyst weight for maximum degradation efficiency ensures that minimal material is used while achieving high efficiency. Furthermore, the equation facilitates the scaling-up of photodegradation processes, making it applicable for real-world wastewater treatment applications. The Polynomial Regression fit obtained for the degradation rate of these acids is presented in Figure 11.

The present study successfully establishes a polynomial regression model that predicts the photodegradation rate of carboxylic acids based on acid type, reaction time, and catalyst weight. The developed equation provides an effective mathematical tool for optimizing reaction conditions and scaling up degradation processes. The results indicate that catalyst weight has the strongest influence on degradation, while acid type and time also play significant roles. Future improvements using machine learning models will further refine predictive accuracy and expand applicability to more complex degradation studies.

This predictive approach helps in optimizing catalyst consumption, reducing material costs while ensuring maximum degradation efficiency.

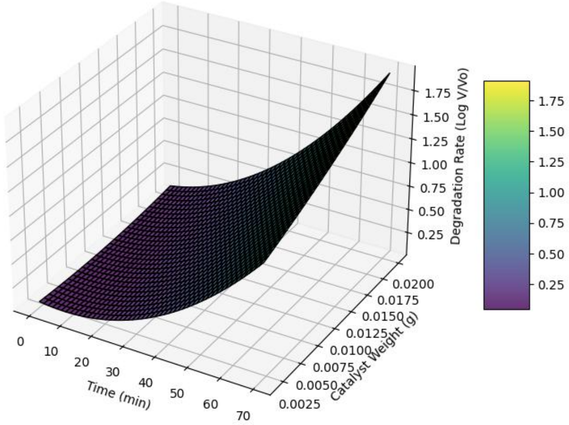

Figure 11. Polynomial Regression model for Degradation rate.

Reusability and regeneration

The fresh NiO_2/MoO_2 photocatalyst exhibited a remarkable degradation efficiency of 96% for carboxylic acids. However, successive reuse cycles revealed a gradual decline in photocatalytic performance. This reduction in efficiency is primarily attributed to the aggregation of photocatalyst particles during reuse, which decreases the specific surface area and limits the availability of active catalytic sites. Additionally, carboxylic acids tend to form dimers in aqueous and organic solutions, which adsorb onto the catalyst surface. These dimeric aggregates create a physical barrier on the catalyst surface, obstructing UV light exposure and further diminishing catalytic activity.

Despite the decline in efficiency, the 1st and 2nd reuse cycles showed nearly identical degradation efficiencies, though the reaction rates were slower compared to the fresh catalyst. This consistency indicates that the nanoscale NiO_2/MoO_2 photocatalyst retains significant catalytic activity even after multiple uses. Furthermore, the potential for regeneration and reuse with minimal efficiency loss highlights the material's suitability for sustainable water treatment applications. Implementing effective regeneration techniques, such as thermal treatment or chemical washing, could further enhance the reusability of the catalyst, making it a viable option for large-scale and long-term environmental remediation.

The observed decrease in efficiency of reused photocatalyst samples is a well-documented phenomenon in photocatalysis research. Studies have reported that the photodegradation efficiency of photocatalysts can decline after multiple reuse cycles. For instance, a study on the photocatalytic degradation of methylene blue using TiO_2 observed a decrease in photodegradation efficiency from 90% in the first cycle to 50% in the second cycle, indicating a significant reduction in activity upon reuse. [Sonu et al., 2021]

Similarly, research on g-C_3N_4/W-TiO_2/PVDF membranes for the degradation of sulfamethazine reported an 18% loss in membrane activity after five cycles of photocatalytic degradation [Hamdy et al., 2024]. These findings suggest that the decline in photocatalytic efficiency upon reuse is a common challenge, often attributed to factors such as catalyst aggregation, surface fouling, or structural changes during the photocatalytic process.

Antibacterial Activity

The antibacterial activity of the NiO_2/MoO_2 nanocomposites was evaluated using the Minimum Inhibitory Concentration (MIC) and the disc diffusion method. MIC represents the lowest concentration of an antimicrobial agent that prevents visible microbial growth after incubation. It is widely regarded as the gold standard for determining microbial susceptibility and plays a crucial role in diagnostic laboratories, particularly for identifying unusual resistance patterns. The disc diffusion method, a qualitative approach based on the agar diffusion technique developed by Bauer and Kirby [Bauer et al., 1966], assesses antimicrobial efficacy by measuring the zone of inhibition (ZOI) created around drug-impregnated discs. The extent of this inhibition directly correlates with the effectiveness of the antimicrobial agent.

For this study, three bacterial strains were tested: Bacillus subtilis (MTCC 441), Lactobacillus acidophilus (MTCC 447), and Staphylococcus aureus (MTCC 96). The antibacterial assay followed the standard protocol outlined by incorporating modifications from CLSI guidelines (2012) [Humphries et al., 2018]. The experiment began with the preparation of Mueller-Hinton Agar plates, where approximately 25 mL of molten agar was poured into sterile Petri plates and allowed to solidify. The bacterial strains were cultured for 18 hours, with their optical density (OD) adjusted to 0.6, ensuring uniform growth conditions. A sterile cotton swab was used to evenly spread the bacterial culture across the agar surface.

Following this, discs impregnated with the test drug at varying concentrations (0 µg/mL, 250 µg/mL, 500 µg/mL, 750 µg/mL, and 1000 µg/mL) were carefully placed on the agar surface. Azithromycin (30 µg/mL) was used as the positive control, while plain discs served as negative controls. The plates were incubated at 37°C for 24 hours, allowing for bacterial growth and subsequent evaluation of inhibition zones. The diameter of the ZOI was measured using an antibiotic zone scale, providing quantitative insight into the antimicrobial efficacy of the NiO_2/MoO_2 nanocomposites.

The results of the antibacterial study demonstrated that the nanocomposites exhibited significant antimicrobial efficacy, with ZOI values increasing proportionally with the concentration of the test drug. Among the tested bacterial strains, Lactobacillus acidophilus displayed the largest zones of inhibition across all concentrations, indicating its higher susceptibility to the NiO_2/MoO_2 nanocomposite. The study underscores the potential of these nanocomposites as effective antimicrobial agents, capable of addressing bacterial contamination concerns in various applications. The antibacterial activity of the test samples against the bacterial strains is detailed in Table 6 and visually represented in Figure 12.

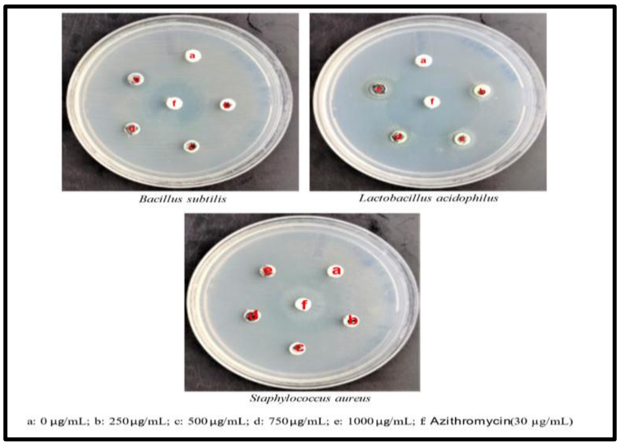

Figure 12. Appearances of inhibitory zones with Bacillus subtilis, Lactobacillusacidophilus and Staphylococcusaureus.

Table 6. Antibacterial effect of NiO_2/MoO_2nanocomposites by Zone of Inhibition (mm) against test strains. (ZOI: Zone of inhibition * Azithromycin)

Name of the Sample	**ZOI(mm)**				**ZOI (mm) Standard**
	0 µg/mL	**250 µg/mL**	**500 µg/mL**	**750 µg/mL**	**30 µg/well**
BacillisSubtilis	**-**	7	8	9	25
Lactobacillus acidophilus	**-**	9	10	11	27
Staphylococcus Aureus	**-**	10	12	14	24

Conclusions

This study successfully demonstrated the synthesis of NiO_2/MoO_2 nanocomposites via an electrochemical method, presenting an effective and sustainable approach for environmental remediation. Comprehensive characterization using UV-Vis spectroscopy, Scanning Electron Microscopy (SEM), Energy Dispersive X-ray Analysis (EDAX), and X-ray Diffraction (XRD) confirmed the structural, morphological, and optical properties of the synthesized nanocomposites, highlighting their potential for catalytic and antimicrobial applications.

The photodegradation efficiency of the NiO_2/MoO_2 nanocomposites was evaluated through the degradation of carboxylic acids, including acetic acid, chloroacetic acid, and trichloroacetic acid. The results showed that the photodegradation process followed first-order kinetics, with degradation rates significantly enhanced under UV light compared to sunlight. The superior photocatalytic performance of the nanocomposites under UV light was attributed to their high charge separation efficiency and optimal band gap energy of 3.83 eV. Chemical Oxygen Demand (COD) measurements verified that approximately 95% of the carboxylic acids were successfully degraded, reinforcing the efficiency of the synthesized material in breaking down persistent pollutants.

In addition to their photocatalytic performance, the NiO_2/MoO_2 nanocomposites demonstrated significant antibacterial activity against Bacillus subtilis, Lactobacillus acidophilus, and Staphylococcus aureus. The antimicrobial assay revealed dose-dependent inhibition zones, with the nanocomposites exhibiting comparable or superior performance to standard antimicrobial agents. This dual functionality—combining photocatalytic and antibacterial properties—positions the NiO_2/MoO_2 nanocomposites as versatile materials for tackling both chemical and biological contaminants in wastewater.

Effectiveness and Future Scope

The synthesized NiO_2/MoO_2 nanocomposites offer a green, cost-effective, and efficient solution for the degradation of organic pollutants and the inhibition of microbial growth. Their high photocatalytic efficiency, driven by the synergistic properties of nickel and molybdenum oxides, underscores their utility in treating industrial effluents and wastewater contaminated with carboxylic acids. Furthermore, their notable antibacterial activity expands their potential to applications in healthcare, such as in antimicrobial coatings or disinfectants.

However, while the laboratory-scale results are promising, further studies are needed to address scalability and practical implementation. Investigations into the regeneration and long-term stability of the nanocomposites, particularly under field conditions, will be essential for their adoption in real-world applications. Additionally, exploring hybrid systems that integrate NiO_2/MoO_2 nanocomposites with other advanced treatment techniques, such as nanofiltration or biological treatments, could enhance their overall efficiency and broaden their applicability.

In conclusion, NiO_2/MoO_2 nanocomposites stand out as multifunctional materials with tremendous potential for environmental remediation and antimicrobial applications, paving the way for sustainable solutions to address global challenges in water purification and public health.

References

Ananda, S., Gowda, N. M. M., & Raksha, K. R. (2014). Synthesis of niobium doped ZnO nanoparticles by electrochemical method: characterization, photodegradation of indigo carmine dye and antibacterial study. Advances in Nanoparticles, 3(04), 133.

Bauer, A. W., Kirby, W. M. M., Sherris, J. C., & Turck, M. (1966). Antibiotic susceptibility testing by a standardized single disk method. American Journal of Clinical Pathology, 45(4_ts), 493–496.

Behbahani, M., Lin, B., Phares, T. L., & Seo, Y. (2018). Understanding the impact of water distribution system conditions on the biodegradation of haloacetic acids and expression of bacterial dehalogenase genes. Journal of Hazardous Materials, 351, 293–300.

Bott, G., Field, L. D., & Sternhell, S. (1980). Steric effects. A study of a rationally designed system. Journal of the American Chemical Society, 102(17), 5618–5626.

Brookes, C., Wells, P. P., Cibin, G., Dimitratos, N., Jones, W., Morgan, D. J., & Bowker, M. (2014). Molybdenum oxide on Fe2O3 core–shell catalysts: probing the nature of the structural motifs responsible for methanol oxidation catalysis. ACS Catalysis, 4(1), 243–250.

Bukkitgar, S. D., Kumar, S., Singh, S., Singh, V., Reddy, K. R., Sadhu, V., Bagihalli, G. B., Shetti, N. P., Reddy, C. V., & Ravindranadh, K. (2020). Functional nanostructured metal oxides and its hybrid electrodes–Recent advancements in electrochemical biosensing applications. Microchemical Journal, 159, 105522.

Exner, O. (1964). On the enthalpy-entropy-relationship. Collection of Czechoslovak Chemical Communications, 29(5), 1094–1113.

Hamdy, N., El-Geundi, M., Fuoad, M., & Alalm, M. G. (2024). Optimization and reusability of photocatalytic g-C3N4/W-TiO2/PVDF membranes for degradation of sulfamethazine. Environmental Science and Pollution Research, 1–16.

Hu, S., Sun, X., Liu, Z., Gao, L., Li, X., Yu, C., Han, X., Xie, J., & Sun, X. (2024). Annealing activated nickel–molybdenum oxide as an efficient electrocatalyst toward benzyl alcohol upgrading. Energy Advances, 3(1), 281–286.

Huang, L., Yang, F., Xu, S., & Zhou, S. (2001). Studies of structure and electrocatalytic hydrogen evolution on electrodeposited nanocrystalline Ni-Mo alloy electrodes. Transactions of the IMF, 79(4), 136–139.

Humphries, R. M., Hindler, J. A., Magnano, P., Wong-Beringer, A., Tibbetts, R., & Miller, S. A. (2018). Performance of ceftolozane-tazobactam Etest, MIC test strips, and disk diffusion compared to reference broth microdilution for β-lactam-resistant Pseudomonas aeruginosa isolates. Journal of Clinical Microbiology, 56(3), 10–1128.

Khan, S. H., Pathak, B., & Fulekar, M. H. (2017). Spherical Surfaced Magnetic (Fe3O4) Nanoparticles as Nano Adsorbent Material for Treatment of Industrial Dye Effluents. International Journal of Nanoscience and Nanotechnology, 13(2), 169–175.

Kondawar, S., Mahore, R., Dahegaonkar, A., & Agrawal, S. (2011). Electrical conductivity of cadmium oxide nanoparticles embedded polyaniline nanocomposites. Advances in Applied Science Research, 2(4), 401–406.

Lewis, J. M., Kydd, R. A., Boorman, P. M., & van Rhyn, P. H. (1992). Phosphorus promotion in nickel-molybdenum/alumina catalysts: model compound reactions and gas oil hydroprocessing. Applied Catalysis A: General, 84(2), 103–121.

Li, M. M.-J., Ye, L., Zheng, J., Fang, H., Kroner, A., Yuan, Y., & Tsang, S. C. E. (2016). Surfactant-free nickel–silver core@ shell nanoparticles in mesoporous SBA-15 for chemoselective hydrogenation of dimethyl oxalate. Chemical Communications, 52(12), 2569–2572.

Liu, Z., Zhang, Z., Peng, J., Wu, J., & Huo, Y. (2022). Rapid removal of trace haloacetic acids from drinking water by a continuous adsorption process using graphene oxide. Environmental Technology, 43(10), 1544–1550.

Ma, X., Lu, G., & Yang, B. (2002). Study of the luminescence characteristics of cadmium sulfide quantum dots in a sulfonic group polyaniline (SPAn) film. Applied Surface Science, 187(3–4), 235–238.

Ma, Z., Meng, H., Wang, M., Tang, B., Li, J., & Wang, X. (2018). Porous Ni− Mo− S Nanowire Network Film Electrode as a High-Efficiency Bifunctional Electrocatalyst for Overall Water Splitting. ChemElectroChem, 5(2), 335–342.

Majewski, A. J., Wood, J., & Bujalski, W. (2013). Nickel–silica core@ shell catalyst for methane reforming. International Journal of Hydrogen Energy, 38(34), 14531–14541.

Mamatha, K. M., Ravikumar, C. R., Murthy, H. C. A., Kumar, V. G. D., Kumar, A. N., & Jahagirdar, A. A. (2022). Facile green synthesis of Molybdenum oxide nanoparticles using Centella Asiatica plant: Its photocatalytic and electrochemical lead sensor applications. Sensors International, 3, 100153.

Manivel, A., Lee, G.-J., Chen, C.-Y., Chen, J.-H., Ma, S.-H., Horng, T.-L., & Wu, J. J. (2015). Synthesis of MoO3 nanoparticles for azo dye degradation by catalytic ozonation. Materials Research Bulletin, 62, 184–191.

McRae, B. M., LaPara, T. M., & Hozalski, R. M. (2004). Biodegradation of haloacetic acids by bacterial enrichment cultures. Chemosphere, 55(6), 915–925.

Pan, S., An, W., Li, H., Su, M., Zhang, J., & Yang, M. (2014). Cancer risk assessment on trihalomethanes and haloacetic acids in drinking water of China using disability-adjusted life years. Journal of Hazardous Materials, 280, 288–294.

Punyapalakul, P., Soonglerdsongpha, S., Kanlayaprasit, C., Ngamcharussrivichai, C., & Khaodhiar, S. (2009). Effects of crystalline structures and surface functional groups on the adsorption of haloacetic acids by inorganic materials. Journal of Hazardous Materials, 171(1–3), 491–499.

Raj, I. A., & Vasu, K. I. (1990). Transition metal-based hydrogen electrodes in alkaline solution—electrocatalysis on nickel based binary alloy coatings. Journal of Applied Electrochemistry, 20(1), 32–38.

Rajput, A., Rahman, M. A., Rahman, M. H., & Kuila, A. (2024). Visible light photocatalytic degradation of organic pollutants in industrial wastewater by engineered TiO2 nanoparticles. Biomass Conversion and Biorefinery, 14(15), 17301–17311.

Sanches, L. S., Domingues, S. H., Marino, C. E. B., & Mascaro, L. H. (2004). Characterisation of electrochemically deposited Ni–Mo alloy coatings. Electrochemistry Communications, 6(6), 543–548.

Shilpa, R., Kumar, H. C. C., & Ananda, S. (2020). Synthesis of CdS Nanoparticles by Electrochemical Method: Correlation for Photodegradation of Trichloroacetic Acid, Chloroacetic Acid, Acetic Acid and Antibacterial Efficiency. Journal of Nanoscience and Technology, 874–878.

Shorter, J. (1978). Multiparameter extensions of the Hammett equation. In Correlation Analysis in Chemistry: Recent Advances (pp. 119–173). Springer.

Solomon, G., Landström, A., Mazzaro, R., Jugovac, M., Moras, P., Cattaruzza, E., Morandi, V., Concina, I., & Vomiero, A. (2021). NiMoO4@ Co3O4 core–shell nanorods: in situ catalyst reconstruction toward high efficiency oxygen evolution reaction. Advanced Energy Materials, 11(32), 2101324.

Sonu, K., Puttaiah, S. H., Raghavan, V. S., & Gorthi, S. S. (2021). Photocatalytic degradation of MB by TiO2: studies on recycle and reuse of photocatalyst and treated water for seed germination. Environmental Science and Pollution Research, 28(35), 48742–48753.

Tang, S., Wang, X., Yang, H., & Xie, Y. F. (2013). Haloacetic acid removal by sequential zero-valent iron reduction and biologically active carbon degradation. Chemosphere, 90(4), 1563–1567.

Tari, F., Manteghian, M., & Tazarv, S. (2018). Synthesis of Nickel/Molybdenum Oxide Bimetallic Nanoparticles via Microwave Irradiation Technique. International Journal of Nanoscience and Nanotechnology, 14(1), 57–64.

Tung, H., Unz, R. F., & Xie, Y. F. (2006). HAA removal by GAC adsorption. Journal-American Water Works Association, 98(6), 107–112.

Uma, B., Anantharaju, K. S., Renuka, L., Malini, S., More, S. S., Vidya, Y. S., & Meena, S. (2021). Synthesis of CuO samples by co-precipitation and green mediated combustion routes: Comparison of their structural, optical properties, photocatalytic, antibacterial, haemolytic and cytotoxic activities. Ceramics International, 47(7), 10355–10369.

Urs, G. T., Byrappa, K., & Somashekar, R. (2016). Effect of microwave irradiation on the microstructural properties of bivoltine silk fibroin films. Procedia Engineering, 141, 53–58.

https://doi.org/10.5281/zenodo.17713701

Urs, G. T., Prakash, M. B. N., Ananda, H. T., & Somashekar, R. (2014). Radial distribution studies on water soluble polymers using XRD line profile data. AIP Conference Proceedings, 1591(1), 170–171.

Urs, T. G., Gowtham, G. K., Nandaprakash, M. B., Mahadevaiah, D., Sangappa, Y., & Somashekar, R. (2017). Determination of force constant and refractive index of a semiconducting polymer composite using UV/visible spectroscopy: a new approach. Indian Journal of Physics, 91, 53–56.

Vidales, A. G., & Semai, M. (2023). Platinum nanoparticles supported on nickel-molybdenum-oxide for efficient hydrogen production via acidic water electrolysis. Journal of Molecular Structure, 1290, 135956.

Videa, M., Crespo, D., Casillas, G., & Zavala, G. (2010). Electrodeposition of nickel-molybdenum nanoparticles for their use as electrocatalyst for the hydrogen evolution reaction. Journal of New Materials for Electrochemical Systems, 13(3), 239–244.

Villanueva, C. M., Cantor, K. P., Cordier, S., Jaakkola, J. J. K., King, W. D., Lynch, C. F., Porru, S., & Kogevinas, M. (2004). Disinfection Byproducts and Bladder Cancer: A Pooled Analysis. Epidemiology, 15(3). https://journals.lww.com/epidem/fulltext/2004/05000/disinfection_byproducts_and_bladder_cancer__a.21.aspx

Wang, K., Guo, J., Yang, M., Junji, H., & Deng, R. (2009). Decomposition of two haloacetic acids in water using UV radiation, ozone and advanced oxidation processes. Journal of Hazardous Materials, 162(2–3), 1243–1248.

Wei, L., Shifu, C., Wei, Z., & Sujuan, Z. (2009). Titanium dioxide mediated photocatalytic degradation of methamidophos in aqueous phase. Journal of Hazardous Materials, 164(1), 154–160.

Yang, L., She, Q., Wan, M. P., Wang, R., Chang, V. W.-C., & Tang, C. Y. (2017). Removal of haloacetic acids from swimming pool water by reverse osmosis and nanofiltration. Water Research, 116, 116–125.

Yang, L., Zhou, J., She, Q., Wan, M. P., Wang, R., Chang, V. W.-C., & Tang, C. Y. (2017). Role of calcium ions on the removal of haloacetic acids from swimming pool water by nanofiltration: mechanisms and implications. Water Research, 110, 332–341.

Zhao, X., Li, A., Mao, R., Liu, H., & Qu, J. (2014). Electrochemical removal of haloacetic acids in a three-dimensional electrochemical reactor with Pd-GAC particles as fixed filler and Pd-modified carbon paper as cathode. Water Research, 51, 134–143.

Acknowledgements:

The authors sincerely thank PES College of Engineering, Mandya, for their continuous support and encouragement in facilitating this research.

Funding: Not applicable (N/A).

Authors’ Contributions:

- **Charan Kumar H. C.:** Original idea and manuscript drafting.
- **Shilpa R. and Thejas Urs G.:** Sample preparations and data acquisition.
- **Raghavendra M. P.:** Antibacterial studies.
- **Harsha M.:** Conceptualization, data interpretation and final manuscript editing.

Ethical Approval: Not applicable (N/A).

Consent to Participate: Not applicable (N/A).

Consent to Publish: Not applicable (N/A).

Competing Interests: The authors declare no competing interests.

Data Availability Statement: Data will be made available upon reasonable request.

Received: Oct 23, 2025 **Accepted:** Nov 23, 2025 **Published:** Nov 25, 2025